Chiral mononuclear lanthanide complexes derived from chiral Schiff bases: Structural and magnetic studies

J. Mayans [a,*], L. Sorace [b,*], M. Font-Bardia [c,d], A. Escuer [a]

a Departament de Química Inorgànica i Orgànica, Secció Inorgànica and Institut de Nanociència i Nanotecnologia (IN2UB), Universitat de Barcelona, Martí i Franqués 1-11, Barcelona 08028, Spain
b Dipartimento di Chimica ''Ugo Schiff'' & INSTM RU, Università degli Studi di Firenze, Via della Lastruccia 3, 50019, Sesto Fiorentino (Firenze), Italy
c Departament de Mineralogia, Cristal·lografia i Dipòsits Minerals, Universitat de Barcelona, Martí Franqués s/n, Barcelona 08028, Spain
d Unitat de Difracció de R-X. Centre Científic i Tecnològic de la Universitat de Barcelona (CCiTUB), Solé i Sabarís 1-3, Barcelona 08028, Spain

julia.mayans@qi.ub.edu (J. Mayans).

47 **ABSTRACT:**

48

49 A new family of mononuclear lanthanide complexes with formula [LnIII(L)Cl3] (Ln = Eu (1), Tb (2),

50 Dy (3), Er (4), Yb (5)) and L = N,N0-bis((1,2-diphenyl-(pyridine-2-yl)methylene)-(R,R/S,S)-ethane-1,2-

51 diamine has been obtained employing enantiomerically pure Schiff bases. The complexes have been

52 structurally characterized using X-ray single crystal and powder diffraction. Their dynamic magnetic

53 properties have been studied showing that this family presents slow relaxation of the magnetization

54 under certain conditions and confirms the different behavior of each LnIII cations in isostructural

55 complexes: only the Er one possibly relaxing via an overbarrier Orbach process, while Raman process

56 dominates for Dy and Yb derivative.

57

58

1. INTRODUCTION

Coordination chemistry related with lanthanide cations has been experiencing an increasing impact since the discovery in 2003 by Ishikawa and co-workers [1] that a terbium–phthalocyaninate complex is magnetically bistable up to 30 K. This potentially opened new way to molecular-based magnetic memory unit and spurred a large wealth of studies. It was soon realized that this somehow surprising magnetic behavior is due to the large magnetic moment of TbIII ($7F6$) and to the strong easy axis type single ion anisotropy which it assumes in the specific coordination environment [2–5]. This results in a large barrier to the reorientation of the magnetization which can be overcome by an Orbach-type thermally activated process, with a relaxation time that obeys the Arrhenius law. Following this first report, hundreds of lanthanide- based complexes have been reported to show slow relaxation of the magnetization, as probed by ac susceptometry, either with or without an external applied field [3,6–10]. Among this, DyIII based complexes have been by large the most studied lanthanide ones due to the large magnetic moment of DyIII and to its Kramers ion nature, which ensures a strict degeneracy of the two lowest lying levels and reduce the possibility of magnetization relaxation via Quantum Tunneling of the Magnetization. It is however clear, that any lanthanide ions (with the obvious exception of EuIII) can show slow relaxation of the magnetization in specific cases. Theoretical and experimental studies have shown that a key role is played by the symmetry of the crystal fields around the lanthanide cation which could effectively enhance the ion anisotropy [11,12]. In the past few years, however, many reports pointed out that the presence of a large anisotropy barrier is not enough to increase the relaxation time in all the temperature range, due to the competing relaxation mechanisms, such as Raman and direct one [13,14].

Lanthanide based complexes are specifically interesting in luminescence investigations due to their characteristic narrow line-like emissions, long lifetimes and high quantum yields. When this luminescence is mixed with chirality by using enantiopure organic ligands new optical properties can be found in the synthesized systems, related to absorption and to emission, which can be studied spectroscopically with Electronic Circular Dichroism (ECD) and Circularly Polarized Luminescence (CPL), respectively. While the ECD allows to confirm the enantiopurity of a compound and confirms the stabilization (or not) of a complex in the solid state and in solution, the presence of polarized emission (CPL) can be useful for applications in materials and bioscience fields using the compounds as biomarkers and biosensors [15–19].

Following this reasoning, for this work we have synthesized a new family of mononuclear compounds derived from the chiral Schiff base ligand N,N0-bis((1,2-diphenyl-(pyridine-2-yl)methylene)-(R,R/S,S)-ethane-1,2-diamine (Scheme 1) obtained from the condensation of two equivalents of 2-pyridinecarboxaldehyde with one equivalent of (1R, 2R/1S, 2S)-diphenylethylenediamine in methanolic solution with general formula [LnIII(L)Cl3] (LnIII = Eu (1), Tb (2), Dy (3), Er (4), Yb (5)). All of these compounds present slow relaxation of the magnetization under an applied external bias field with the

96   exception of TbIII and EuIII derivative. For complex 4, we also measured the diluted compound which

97   was also prepared, exploiting as dilution media the isostructural EuIII based complex (4b), which has a

98   non-magnetic ground state. This dilution allowed us to observe the hyperfine coupling in the Electronic

99   Paramagnetic Resonance (EPR) spectrum of the ErIII and to draw some conclusions about the different

100   processes influencing the relaxation dynamics.

101

102 **2. EXPERIMENTAL**

103

104 2.1. Physical measurements.

105

106 Ac susceptibility measurements were carried out on polycrystalline samples in a Quantum Design PPMS

107 on microcrystalline powdered samples pressed in a pellet to avoid field-induced orientations.

108 Diamagnetic corrections were calculated using Pascal's constants. Infrared spectra (4000–400 cm^{-1})

109 were recorded from KBr pellets on a Bruker IFS-125 FT-IR spectrophotometer. ECD spectra were

110 measured on a Jasco-815 spectropolarimeter by preparing a methanolic solution which was poured into

111 1 cm path length quartz cuvettes and diluted until obtaining an adequate concentration. X-band (ν ≈

112 9.45 GHz) EPR spectrum of complex 4b was recorded in a commercial Bruker E500 spectrometer

113 equipped with a continuous 4He flow ESR900 (Oxford Instruments) for low temperature measurements.

114

115 2.2. Syntheses

116 Synthesis of L. The ligand solution of the Schiff base L was employed directly to synthesize the

117 corresponding complexes 1–5 without isolation of the solid ligand. The syntheses of the ligands were

118 common for the (RR) and for the (SS) enantiomers: 0.053 g (0.5 mmol) of 2-pyridinecarboxaldehyde

119 and 0.053 g (0.25 mmol) of (1R, 2R/1S, 2S)-diphenylethylenediamine were dissolved in 20 mL of

120 methanol and stirred at room temperature for three hours.

121 [Ln(RR-L)2Cl6] and [Ln(SS-L)2Cl6] for all the lanthanide cations and were synthesized following the

122 same procedure and just changing the corresponding enantiopure ligand and the corresponding

123 lanthanide chloride. 20 mL (0.25 mmol) of the previously prepared solution of the ligand (L) were

124 added to an equimolar quantity of a LnCl3·nH2O methanolic solution (10 mL). The resulting solution

125 was stirred for one hour at room temperature. Crystals suitable for monocrystal X-ray diffraction in the

126 shape of white needles were obtained a few days later by slow diffusion with diethyl ether. Anal.

127 Calc./found for 2RR (C26H22Cl3N4Tb): C, 47.62/47.2, N, 8.54/8.7; H, 3.38/3.5. IR spectra for 2RR

128 and 2SS compounds (cm^{-1}) as an example for the 1–5 series (Fig. S1).

129

3. CRYSTALLOGRAPHIC MEASUREMENTS

White needles specimens of (2RR) and (2SS) were used for the monocrystal X-ray crystallographic analysis. The X-ray intensity data were measured on a D8 Venture system equipped with a multilayer monochromator and a Mo microfocus (k = 0.71073 Å).

The frames were integrated with the Bruker SAINT software package using a narrow-frame algorithm. The structures were solved and refined using the Bruker SHELXTL Software Package. Crystal data and refinement details are summarized in Table 1. Powder X-ray diffractions were performed in a PANalytical X'Pert PRO MPD h/h powder diffractometer of 240 mm of radius, in a configuration of convergent beam with a focalizing mirror and a transmission geometry with flat samples sandwiched between low absorbing films and Cu Ka radiation (k = 1.5418 nm).

4. RESULTS AND DISCUSSION

4.1. Structural description

Only complexes 2RR and 2SS were solved by single crystal Xray diffraction (the TbIII derivatives) whereas the other complexes were characterized by Powder-X-ray diffraction. The structures of complexes 2RR and 2SS show a mononuclear neutral complex of TbIII whose crystalline system is triclinic (Fig. 1). In the unit cell there are four non-equivalent molecules (labelled A–D) with similar bond parameters. These four molecules differ only slightly in the bond distances and angles. The further data reported in Table 2 refer to molecules A.

In complex 2, the terbium cation is heptacoordinated and its coordination sphere is a pentagonal bipyramid. First, TbIII is coordi- nated to the tetradentate ligand L, which occupies the equatorial positions of the complex. The linkage of the metal with the ligand is via the four N-donors of the ligand, that form Npy–Tb–Nimine angles much lower than 90⧠ due to the small bite of the ligand, ranging from 64.4⧠ to 64.8⧠ in the case of complex 2SS, while in the case of 2RR they range from 64.2⧠ to 65.5⧠ (see Table 2). In both cases, the coordination of L leaves enough free space around the ion to coordinate the chloride ligand as fifth donor in the same plane.

The coordination sphere is completed by two additional chloride ligands occupying the axial positions, forming a Cl1–Tb1–Cl2 bond angle close to 180⧠. In compound 2SS, the stated angle is 172.0⧠ and for compound 2RR, 167.8⧠. CShM value calculate with SHAPE [20,21] is 1.36 indicating an almost perfect BPP environment.

There are no relevant intermolecular hydrogen bonds as a consequence of the lack of crystallization solvents, O-donors or accessible N atoms. The only intermolecular interactions are promoted by weak CH⧠ ⧠ ⧠ Cl contacts between the coordinated chloro ligands and the nearest H-atoms from pyridinic fragments of the nearby molecule with Cl⧠ ⧠ ⧠ Cl distances around 3.5 Å which optimizes the maximum possible packing.

The powder X-ray diffraction spectra for the complete series of mononuclear Ln complexes 1–5 (Fig. 2), show a complete agreement of the experimental diffraction patterns with the spectrum calculated from the single crystal structure of compounds 2, evidencing that compounds 1–5 are isostructural. The lack of crystallization solvents results in stable crystals at ambient conditions [22].

4.2. UV–Visible spectrum and Electronic Circular Dichroism Spectroscopies

The UV–Visible spectra (Fig. 3) were collected using samples from the ligand L and compound 2 in methanolic solutions. UV–Vis spectra are dominated by the transitions related to the ligand in the 200–325 nm range with one absorption at 206 nm due to the p–p* transition of the aromatic ring and another

band at 215 nm (265 nm shoulder) related to the iminic group. For complex 4, the transition at 205 nm is maintained while the other one is shifted to 300 nm; however, bands corresponding to the LnIII atoms transitions were not observed.

ECD spectra of the enantiomeric pair of pure 2RR and 2SS complexes were measured in methanolic solutions and are mirror images of one another as should be expected for a pair of enantiomers, Fig. 4. The two CD spectra are similar since the bands that are observed are due to the p–p* transitions of the ligand L. The chirality around the metal cation is not observed in this case due to the low chirality transfer from ligand to metal.

4.3. Dynamic magnetic properties

A few families of pentagonal bipyramidal complexes have been reported in recent years to show very high barrier to the relaxation of the magnetization [23,24]. We then investigated the dynamic magnetic properties of complexes 2–5 by ac susceptometry. No maxima appear in the v00 vs. T measurements above 1.8 K at zero field for any of the compounds; and no maxima appear under any dc applied field for complex 2 probably due its non-Kramers nature, which makes Quantum Tunneling of the magnetization extremely efficient.

For the DyIII derivative, 3, a dc field of 1000 G was selected to perform the measurements after a preliminary study of the outof-phase signal under different fields. Its out-of-phase susceptibility dependence in function of the frequency between 10 and 1488 Hz is reported in Fig. 5, left. The corresponding relaxation times as a function of temperature were extracted by fitting the Cole–Cole plots to an extended Debye relaxation model [25] (see supplementary material, Fig. S2) in the range 1.8–5.0 K, using the CCfit software [26]. This also yielded a quite narrow distribution of the relaxation times, with a decreasing from 0.1 at 1.8 K to 0.05 at 5 K.

It is immediately evident from that large deviation from linearity is observed in the Arrhenius plot (Fig. 5, right), indicating the onset of relaxation mechanisms that are different from the simple Orbach one involving a magnetic anisotropy barrier. In such cases it is now customary to include in the modeling of the relaxation other terms, such as Raman, direct, and quantum tunneling ones, according to:

$$\frac{1}{\tau} = \tau_0^{-1} exp(-\Delta/k_B T) + A_{Ram} T^n + B_{dir} T + C_{QTM}$$

(1)

where the first term represents the over barrier Orbach relaxation, the second one is the Raman relaxation rate, the third is the direct term and the fourth is the quantum tunneling one. Since measurements were taken in applied field to minimize the effect of Quantum tunneling processes we attempted the fit by keeping the fourth term to zero. Interestingly, we could not find any combination

that was able to reproduce the observed behaviour by including an Orbach term. Best fit was then obtained by a combination of Raman and direct relaxation processes, with $A_{Ram} = 1.6 \pm 0.2 \text{ s}^{-1}\text{ K}^{-n}$, $n = 5.7 \pm 0.1$, $B_{dir} = 275 \pm 7 \text{ s}^{-1}\text{ K}^{-1}$. The value of the Raman exponent, despite being smaller than that predicted by the original Orbach theory, falls well within range reported values for molecular based Lanthanide systems [10,27] (Table 3).

The same procedure was applied for Er^{III} complex 4 shows the dependency of the out of phase susceptibility as a function of the frequency under different applied dc fields: in this case the application of different magnetic fields results in a much faster relaxation at fields larger than 1000 G, the maximum in v'' shifting above 10 kHz even at 2 K (see supplementary Fig. S3). This is a clear proof of the relevance of the direct process in determining the relaxation, since the corresponding rate is expected to scale as H^2 and thus to be extremely efficient at high field. A second relaxation process, much slower than the first one and essentially temperature independent, also appears at high field (Fig. S3, 3000 G). Such behavior is not uncommon in lanthanide-based complexes and is usually related to a collective process due to dipolar intermolecular interaction [28]. To reduce them, we prepared a solid solution of the Er^{III} complex in one of its diamagnetic isostructural analogues. The first choice for the magnetic dilution was to prepare the Er@Y derivative with a 5% of Er^{III} in the sample. However, the synthesis was not successful (further trials demonstrated that the Y^{III} complex was not formed) and we decided to use Eu^{III} as a magnetic dilutor (complex 4b), taking into account that this cation has a non-magnetic $^7F_0$ ground state [29]. Fig. S4 shows the susceptibility dependency vs. frequency under applied fields of 500 and 1000 G for the Er@Eu system. The corresponding relaxation times as a function of temperature extracted from fits of the ac susceptibility data for both pure and doped samples in different fields are reported in Fig. 6: two aspects are immediately evident: (i) as expected, the doped sample relaxes slower in the whole temperature range; (ii) even in the small temperature range in which slow relaxation is observed the temperature dependences deviate from linearity of the Arrhenius plot indicating that Orbach process is not the only one also in this case. Here, the use of Eq. (1) by neglecting QT terms provides as best fit the following parameters: $B_{dir} = 89 \pm 13 \text{ s}^{-1}\text{ K}^{-1}$, $s_0 = 3 \pm 2 \times 10^{-8} \text{ s}^{-1}$, $D = 40.6 \pm 1.2$ K for Er@Eu. We note that a fit of similar quality could be obtained by excluding Orbach process and assuming contributions from Raman and direct ones, but the best fit value for the n exponent of Raman term is outside of the usually accepted range for this type of systems ($n = 13.6 \pm 0.1$). Furthermore, no fit of the dynamic behaviour of the pure sample could be obtained by including Raman and direct process, while Orbach and direct provided a reasonable fit for these data (best fit parameters: $B_{dir} = 2331 \pm 17 \text{ s}^{-1}\text{ K}^{-1}$, $s_0 = 7.3 \pm 0.3 \times 10^{-10} \text{ s}^{-1}$, $D = 31.7 \pm 0.2$ K) (Table 3).

The magnetic dilution of the complex was also instrumental in obtaining a well-defined Electron Paramagnetic Resonance (EPR) spectrum, compared to the broad one obtained for the pure complex (Fig. S5). The EPR spectrum of 4b is reported in Fig. 7 showing a parallel feature at low field (with signals from $I = 0$ Er isotopes and from ^{167}Er, $I = 7/2$, nat. ab. = 22.9%) and an intense, partially split, perpendicular feature at high field also showing sign of hyperfine coupling.

The spectrum was simulated [30] assuming only the ground doublet to be populated, and an effective spin Hamiltonian:

$$\hat{H}_{Er}^{eff} = \mu_B B \cdot g^{eff} \cdot \hat{S}^{eff} + h\hat{I} \cdot A^{eff} \cdot \hat{S}^{eff}$$

(2)

where the second term represents the hyperfine coupling and has been included only to take into account the contribution of 167Er. Best simulation was obtained with parameters geff x ¼ 1:72 ∓ 0:03, geff y ¼ 2:12 ∓ 0:02, geff z ¼ 14:23 ∓ 0:01 and Aeff x ¼ 400 ∓ 50 MHz, Aeff y ¼ 500 ∓ 50 MHz, Aeff z ¼ 2100 ∓ 200 MHz. Even if the deviation from axiality is far from being negligible we stress here that, to the best of our knowledge, the value for geff z is the highest up to now experimentally measured by EPR in an Er(III) based molecular system [31–33]. This is somehow in agreement with the suggestions of the ac measurements of relaxation occurring predominantly via Orbach process.

For complex 5, the YbIII derivative, the v00 vs. frequency dependence between 10 and 10 000 Hz at different applied magnetic fields are shown in Fig. 8. It is evident that in this case there is essentially no dependence on the applied field of the magnetization dynamics. At the same time, the non-linearity of the corresponding Arrhenius plot, obtained by the fitting of the Argand plots (Fig. S6), indicated also in his case the coexistence of more than one process. The corresponding fit using Eq. (1) and neglecting QTM term provided best fit when using a combination of Raman and direct processes, with the following parameters: ARam = 11.4 ± 0.2 s⁻1 K⁻n, n = 5.38 ± 0.01, Bdir = 1009 ± 6 s⁻1 K⁻1. It is interesting to note that the overall behavior, and the corresponding best fit parameters are close to those obtained for Dy derivative, suggesting that the vibration responsible for this relaxation process are similar in the two cases (Fig. 9, Table 3).

5. CONCLUDING REMARKS

By using enantiomerically pure Schiff bases we obtained a new family of mononuclear lanthanide complexes, in which the lanthanide cation is heptacoordinated with a coordination sphere which is a pentagonal bipyramid.

Their dynamic magnetic characterization demonstrates the presence of slow relaxation of the magnetization for complexes 3, 4 and 5 only under the application of an external magnetic field, probably because of the drawback of relaxation through quantum tunneling due to the largely distorted environments around the cations. This is also in agreement with the fast relaxation of TbIII derivative, which is the only one with an integer spin ground state. Analysis of the temperature dependence of the relaxation points to relaxation occurring via Orbach process with relatively small barrier only for Er derivative, while Dy and Yb are dominated by Raman and direct processes. These are increasingly recognized of major relevance in degrading the performances of lanthanide based SMMs at low temperatures, and their control is actively sought for.

The absence of dominant overbarrier (i.e. Orbach type) relaxation processes is not surprising in this family, since Rinehart-Long model [11] suggests that the type of the anisotropy for the different system has to be different. Indeed, if the coordination geometry around the ion is the same, one would expect that the anisotropy of Yb(III) and of Dy(III), characterized in their highest mJ values by oblate and prolate charge distribution, respectively, should be opposite. In this respect, if one of these were to relax via overbarrier process, the other should not. At the same time the EPR spectrum of Er derivative diluted in Eu evidenced that these systems are characterized by a relevant deviation from axiality, which hampers slow relaxation occurring by overcoming an anisotropy barrier in zero field.

REFERENCES

[1]   N. Ishikawa, M. Sugita, T. Ishikawa, S.Y. Koshihara, Y. Kaizu, J. Am. Chem. Soc. 125 (2003)
        8694.

[2]   J. Tang, P. Zhang, Lanthanide Single Molecule Magnets, Springer-Verlag, Berlin Heidelberg,
        2015, and references herein.

[3]   F. Habib, M. Murugesu, Chem. Soc. Rev. 42 (2013) 3278.

[4]   J.D. Rinehart, M. Fang, W.J. Evans, J.R. Long, Nat. Chem. 3 (2011) 538.

[5]   H.L.C. Feltham, S. Brooker, Coord. Chem. Rev. 276 (2014) 1.

[6]   D.N. Woodruff, R.E.P. Winpenny, R.A. Layfield, Chem. Rev. 113 (2013) 5110.

[7]   B.M. Day, F.S. Guo, R.A. Layfield, Acc. Chem. Res. 51 (2018) 1880.

[8]   Z. Zhu, M. Guo, X.-L. Li, J. Tang, Coord. Chem. Rev. 378 (2019) 350.

[9]   S. Brooker, Coord. Chem. Rev. 276 (2014) 1.

[10]   S.T. Liddle, J. van Slageren, Chem. Soc. Rev. 44 (2015) 6655.

[11]   J.D. Rinehart, J.R. Long, Chem. Sci. 2 (2011) 2078.

[12]   J.-L. Li, Y.-C. Chen, M.-L. Tong, Chem. Soc. Rev. 47 (2018) 2431.

[13]   E. Lucaccini, L. Sorace, M. Perfetti, J.P. Costes, R. Sessoli, Chem. Commun. 50 (2014) 1648.

[14]   K.S. Pedersen, J. Dreiser, H. Weihe, R. Sibille, H.V. Johannesen, M.A. Soerensen, B.E. Nielsen,
        M. Sigrist, H. Mutka, S. Rols, J. Bendix, S. Piligkos, Inorg. Chem. 54 (2015) 7600.

[15]   J. Vuojola, T. Soukka, Methods Appl. Fluoresc. 2 (2014) 012001.

[16]   S. Dang, J.-H. Zhang, Z.-M. Sun, H. Zhang, Chem. Commun. 48 (2012) 11139.

[17]   B. Casanovas, F. Zinna, L. Di Bari, M.S. El Fallah, M. Font-Bardía, R. Vicente, Dalton Trans.
        46 (2017) 6349. [18]   J. Long, Y. Guari, A.S. Ferreira, L.D. Carlos, J. Larionova, Coord.
        Chem. Rev. 363 (2018) 57.

[19]   J.-H. Jia, Q.-W. Li, Y.-C. Chen, J.-L. Lio, M.-L. Tong, Coord. Chem. Rev. (2019) 365.

328 [20]   J. Cirera, P. Alemany, S. Alvarez, Chem. Eur. J. 10 (2004) 190.

329 [21]   SHAPE version 2.0. M. Llunell, D. Casanova, J. Cirera, P. Alemany, S. Alvarez, Barcelona
330   2010.

331 [22]   Kenneth D.M. Harris, Top. Curr. Chem. 315 (2012) 133.

332 [23]   Y.-S. Ding, N.F. Chilton, R.E.P. Winpenny, Y.-Z. Zheng, Angew. Chem., Int. Ed. 55 (2016)
333   16071.

334 [24]   S.K. Gupta, T. Raieshkumar, G. Rajaraman, R. Murugavel, Chem. Sci. 7 (2016) 5181.

335 [25]   D. Gatteschi, R. Sessoli, J. Villain, Molecular Nanomagnets, Oxford University Press, 2016.

336 [26]   The program can be obtained free of charge at http://www.nfchilton.com/ccfit. html.

337 [27]   E. Lucaccini, M. Briganti, M. Perfetti, L. Vendier, J.P. Costes, F. Totti, R. Sessoli, L. Sorace,
338   Chem. Eur. J. 22 (2016) 5552.

339 [28]   R. Orbach, Proc. R. Soc. Lond. A Math. Phys. Sci. 264 (1961) 458.

340 [29]   O. Kahn, Mol. Magnet. (1993).

341 [30]   S. Stoll, A. Schweiger, J. Magn. Reson. 178 (2006) 42.

342 [31]   M.A. AlDaman, S. Cardona-Serra, J.M. Clemente-Juan, E. Coronado, A. Gaita- Arino, C. Marti-
343   Gastaldo, F. Luis, O. Montero, Inorg. Chem. 48 (2009) 3467.

344 [32]   D. Aguila, L.A. Barrios, V. Velasco, O. Roubeau, A. Repolles, P.J. Alonso, J. Sese, S. J. Teat, F.
345   Luis, G. Aromi, J. Am. Chem. Soc. 136 (2014) 14215.

346 [33]   E. Lucaccini, J.J. Baldovi, L. Chelazzi, A.L. Barra, F. Grepioni, J.P. Costes, L. Sorace, Inorg.
347   Chem. 56 (2017) 4728.

348

Legends to figures

Scheme 1. Chart of L ligand used for the synthesis of 1–5 complexes. Asterisk denotes the chiral C-atoms.

Figure. 1 Top, labeled plot of the molecular structure of 2RR (left) and 2SS (right), showing the H-atoms linked to the chiral carbons. Bottom, coordination environment around the terbium cations. The ideal pentagonal bipyramidal polyhedron is depicted in red. (Colour online.)

Figure.2 Powder X-ray diffraction pattern obtained for compounds 1–5 (above) and the calculated spectrum of compound 2 (bottom)..

Figure.3 Representative UV–Vis spectrum for complex 2 and for the ligand L.

Figure.4. Representative ECD spectra for both enantiomers of 2.

Figure.5 Left, representation of the out-of-phase susceptibility for complex 3 in the frequency range 10–1488 Hz. Continuous lines are guides to the eye. Right, Arrhenius plot of complex 3 and best fit obtained using model reported in the text.

Figure.6 Arrhenius plot of the temperature dependence of the magnetization relaxation rate for 4 and 4b in 500 G and 1000 G, respectively. Continuous lines are best fits to the models described in the text.

Figure.7 7. EPR spectrum of the Er@Eu complex at 5 K and best simulation obtained with parameters reported in the text.

Figure.8 v00 vs. frequency plots of YbIII complex 5 at different applied dc fields.

Figure.9 Arrhenius plot of the relaxation time of 5 measured in different applied fields ad corresponding best fit curve using parameters reported in the text. Continuous line represents the fitting of the 1000 G curve.
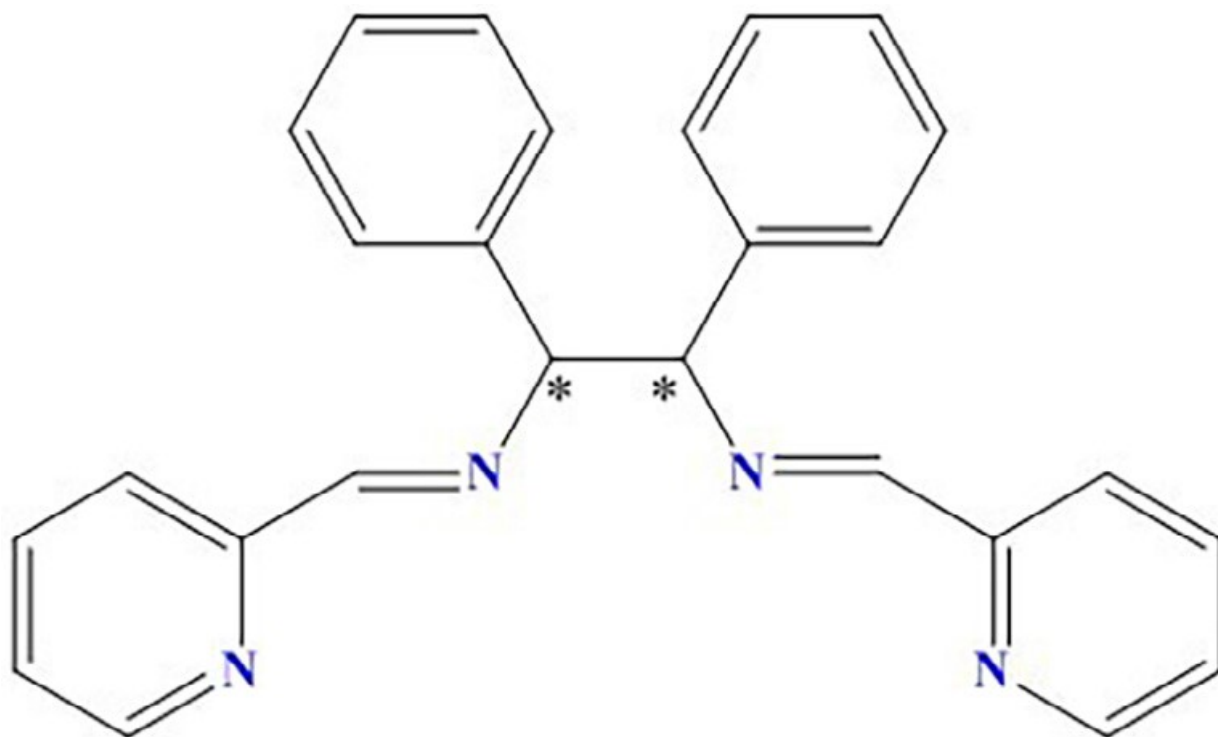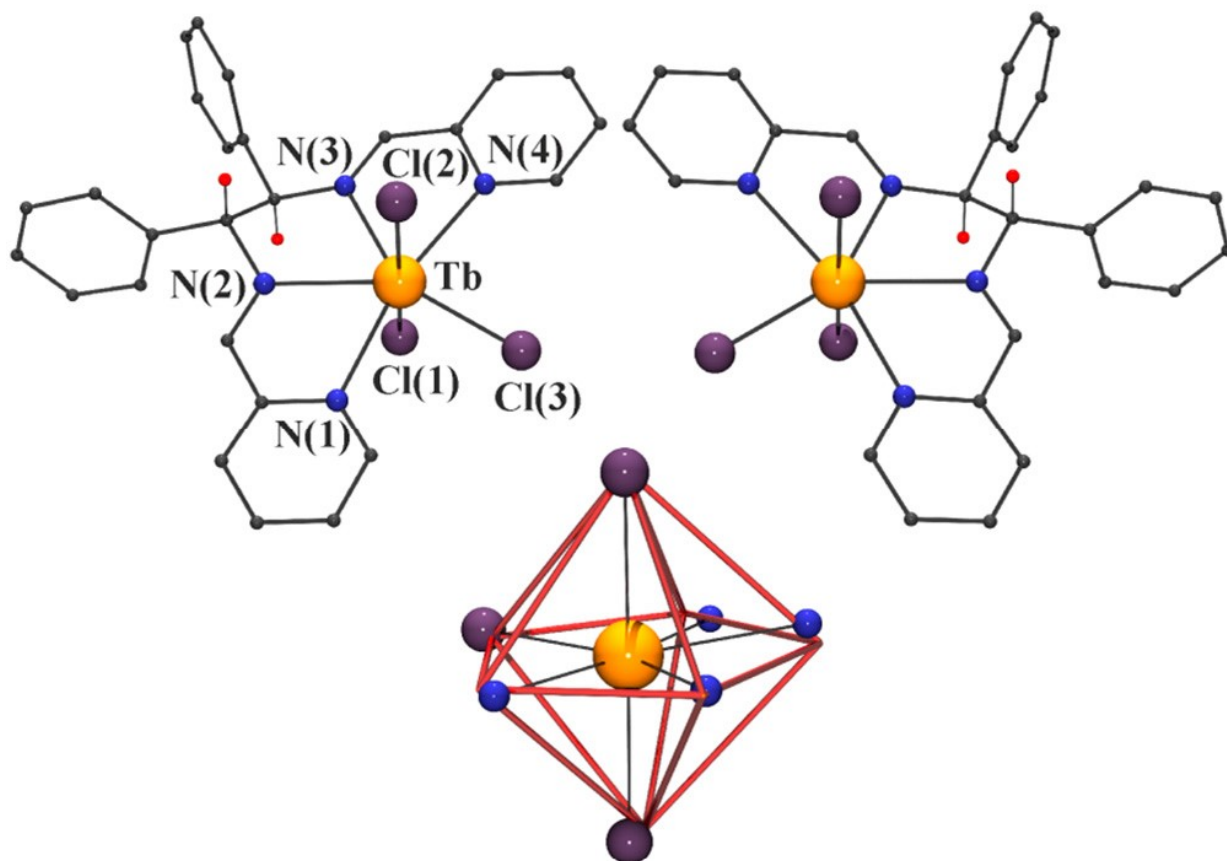
SCHEME 1

FIGURE 1

392

393

394
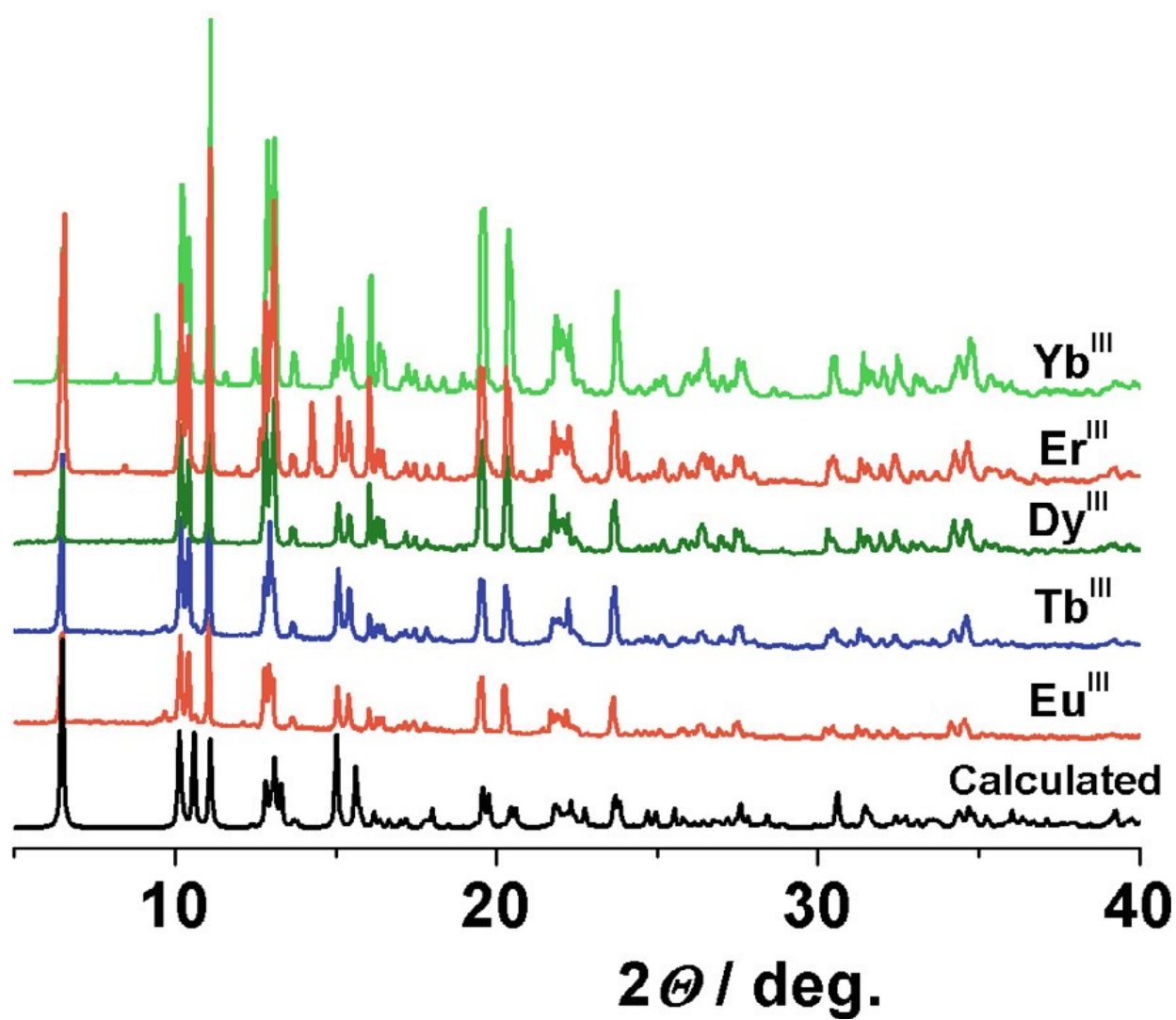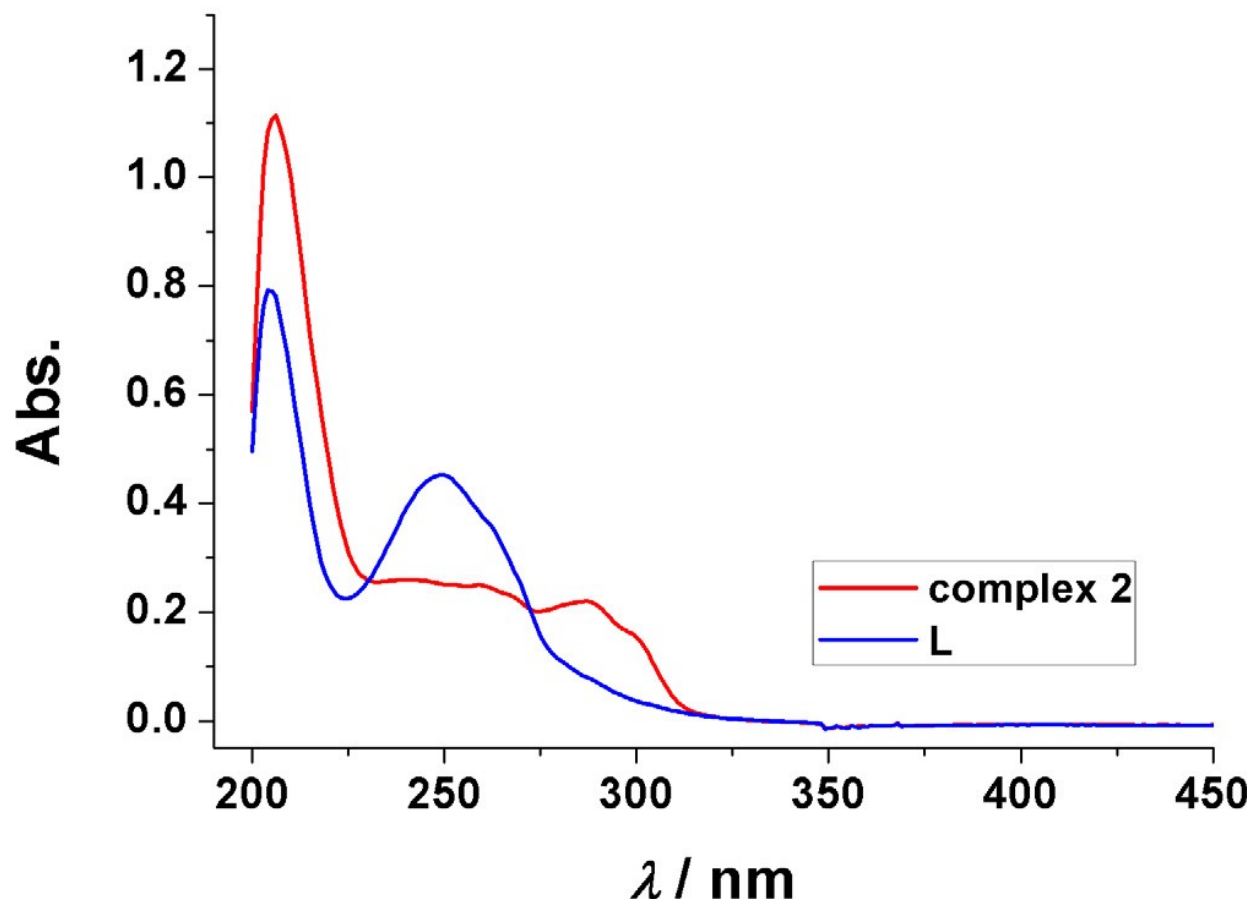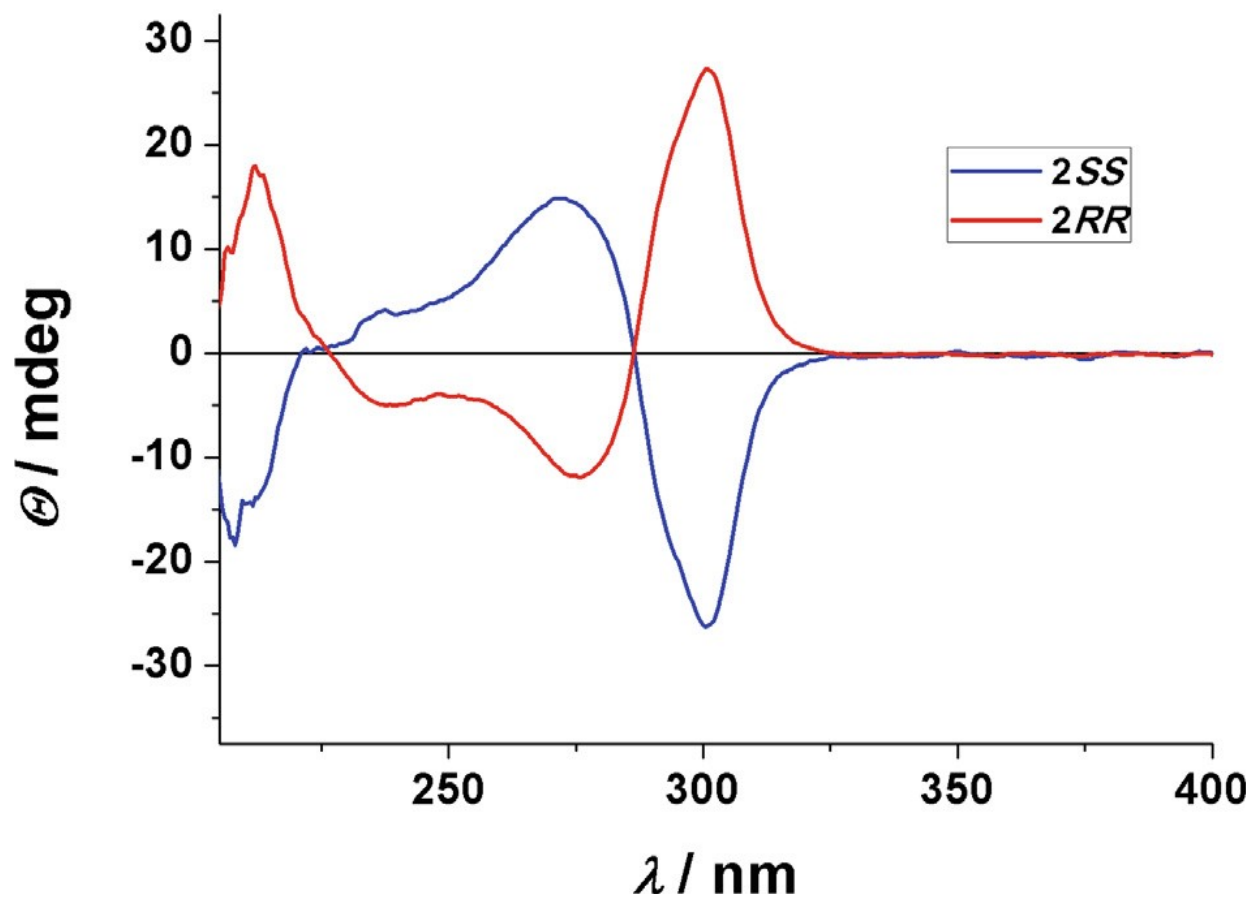
FIGURE 3

FIGURE 4

408 **FIGURE 5**

409

410
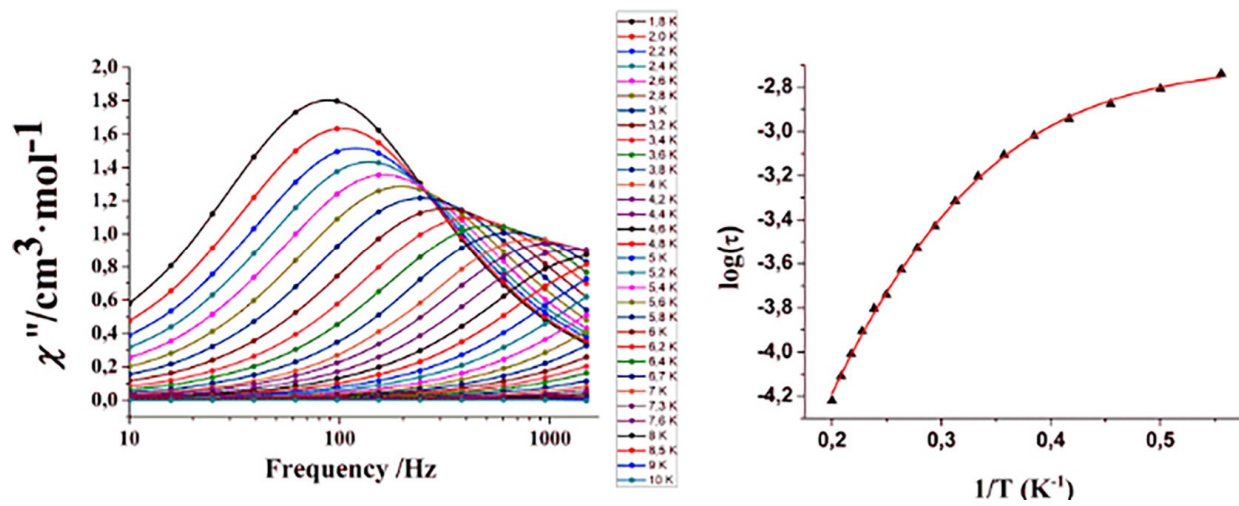
411

412

413

FIGURE 6

414

415
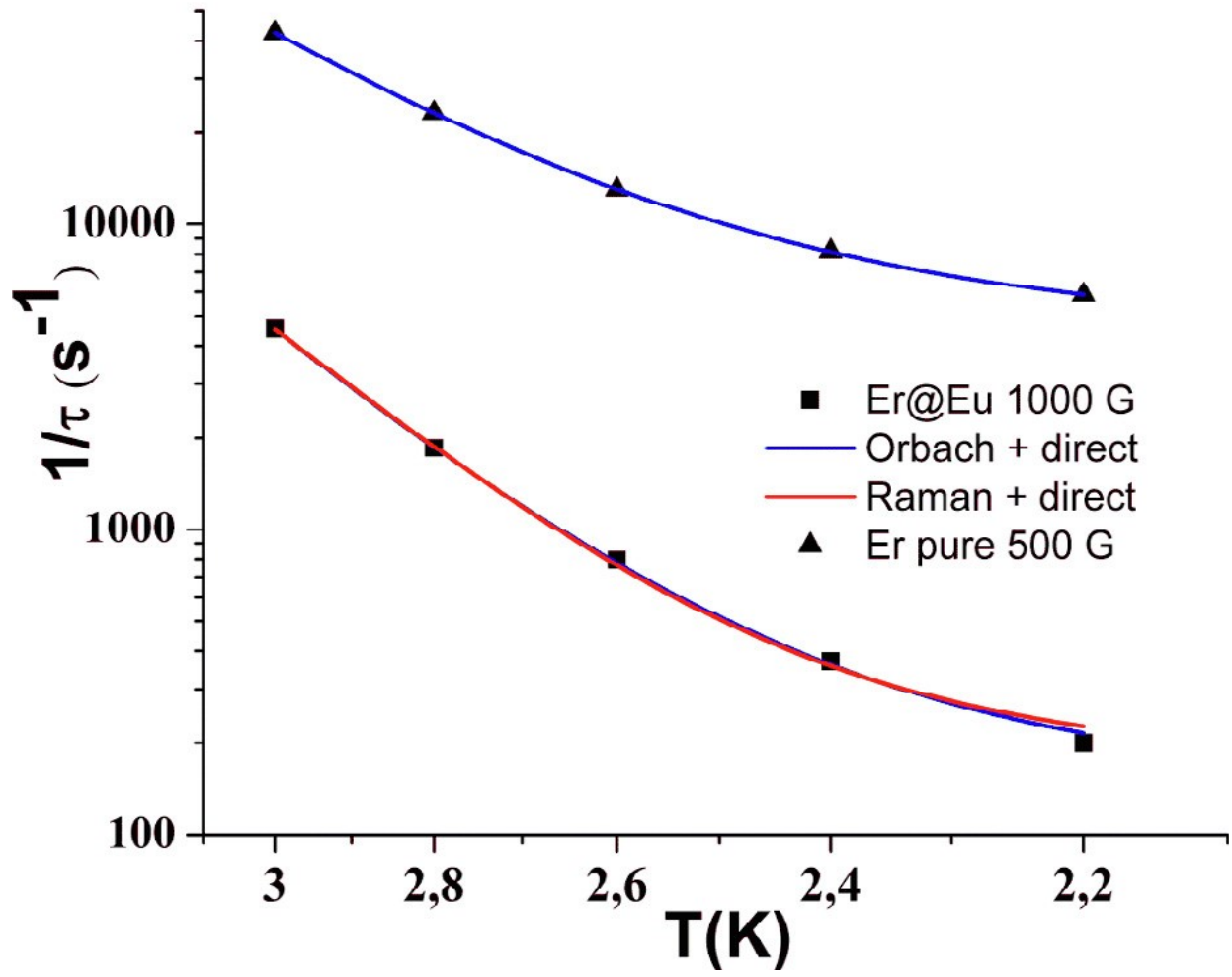
416

417
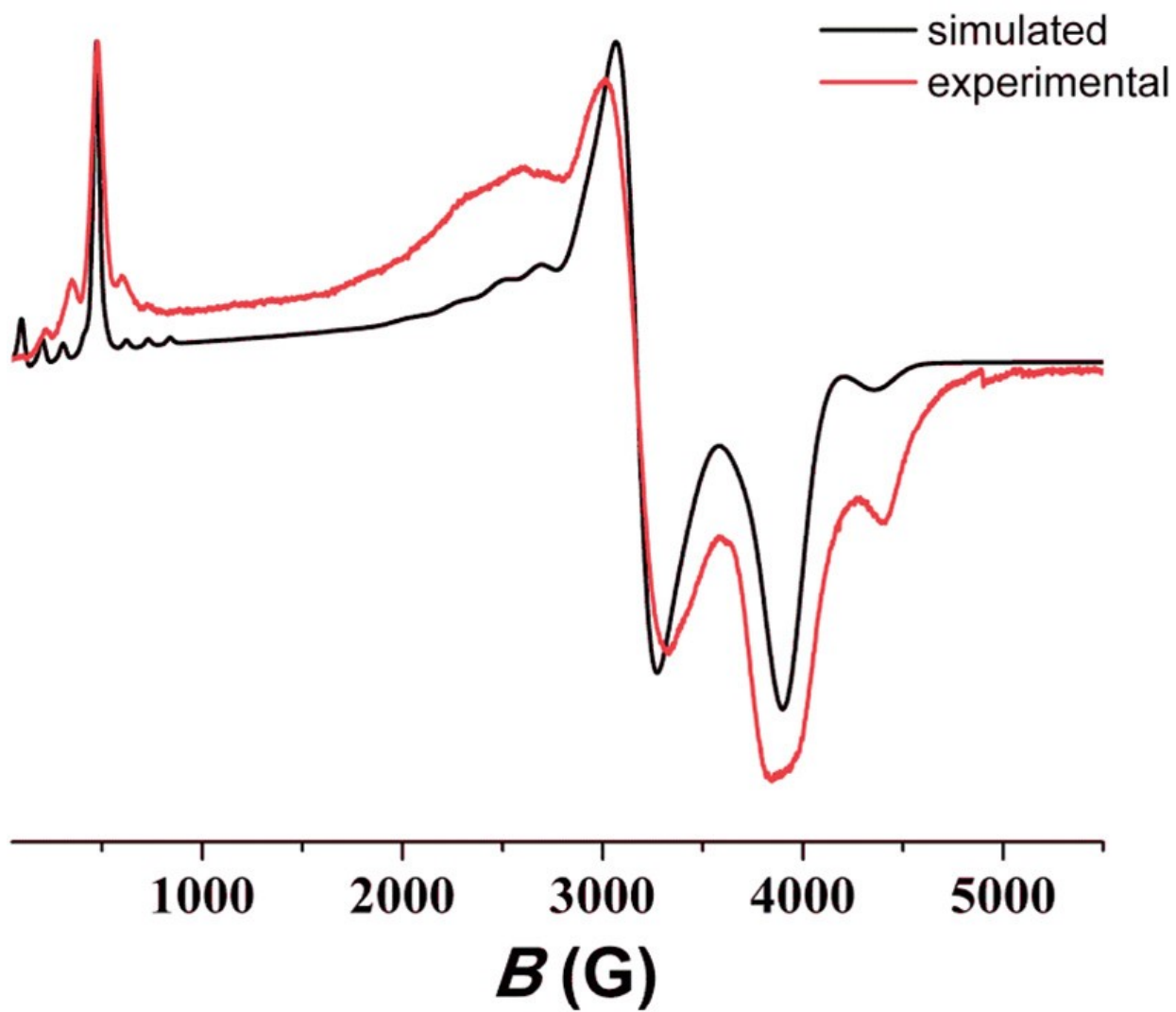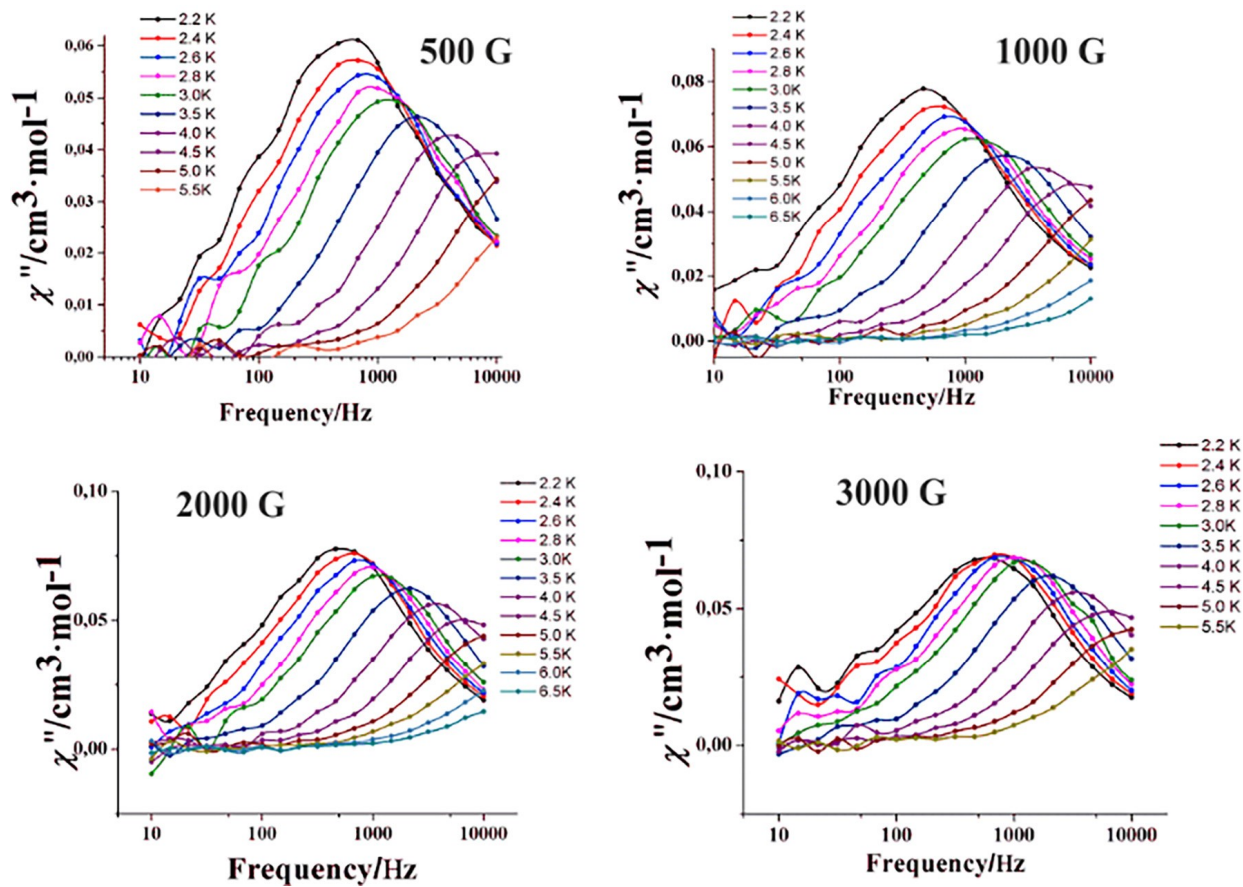
FIGURE 7

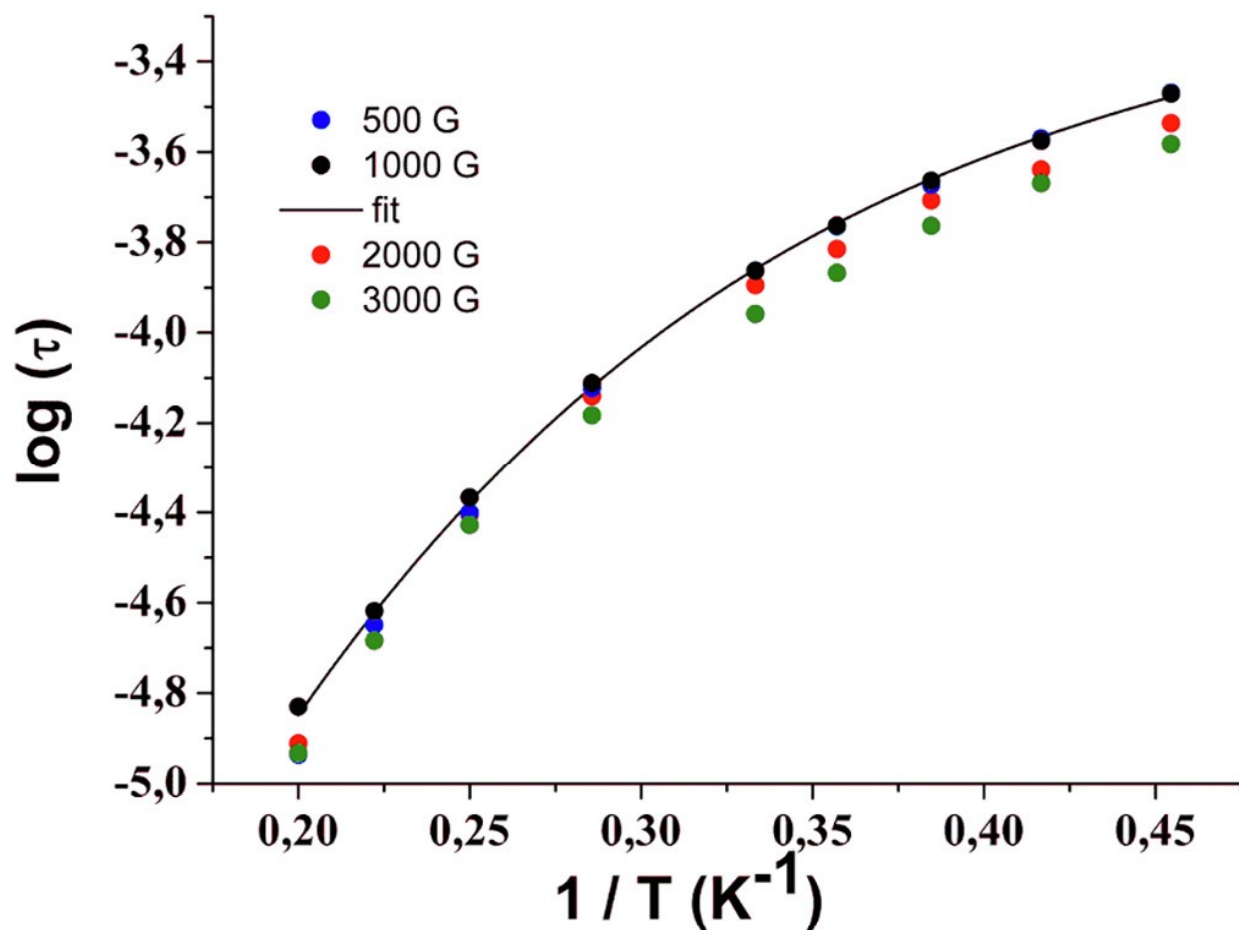**FIGURE 8**

FIGURE 9

433   **Table 1** Crystal data and structure refinement for coordination compounds 1RR and 1SS.

434

	1RR	1SS
Formula	$C_{26}H_{22}Cl_3N_4Tb$	$C_{26}H_{22}Cl_3N_4Tb$
FW	655.74	655.74
System	triclinic	triclinic
Space group	$P\bar{1}$	$P\bar{1}$
a (Å)	8.7672(3)	8.7720(3)
b (Å)	10.9544(5)	10.9600(4)
c (Å)	27.502(1)	27.4997(1)
α (°)	87.262(2)	87.025(2)
β (°)	82.056(2)	81.982(2)
γ (°)	88.241(2)	88.059(2)
V (Å³)	2612.2(2)	2613.5(2)
Z	4	4
T (K)	100(2)	100(2)
λ (Mo Kα) (Å)	0.71073	0.71073
ρ_{calc} (g cm⁻³)	1.667	1.667
μ (Mo Kα) (mm⁻¹)	3.036	3.034
Variables	1226	1063
Maximum/minimum peaks, e Å⁻³	2.210/−1.518	1.200/−1.057
Flack parameter	0.006(5)	0.003(5)
R	0.0236	0.0345
ωR^2	0.0319	0.0539

435

436

437 **Table 2** Selected bond parameters for the A-molecule of the complexes 1RR and 1SS.

438

	1RR – A	1SS – A
Tb1–N1	2.578(5)	2.556(5)
Tb1–N2	2.520(5)	2.513(5)
Tb1–N3	2.521(4)	2.522(5)
Tb1–N4	2.583(6)	2.576(5)
Tb1–C11	2.647(2)	2.632(2)
Tb1–C12	2.609(2)	2.604(2)
Tb1–C13	2.613(2)	2.610(2)
N1–Tb1–N2	63.2(2)	64.4(2)
N2–Tb1–N3	65.5(2)	64.8(2)
N3–Tb1–N4	65.1(2)	64.7(2)
N1–Tb1–C13	83.2(1)	83.5(1)
N4–Tb1–C13	83.4(1)	83.7(1)
C11–Tb1–C12	167.8(4)	172.0(6)

439

440

441 **Table 3** Best fit parameters for the temperature dependencies of the relaxation rates of the investigated

442 family.

443

	A_{Ram} (s^{-1} K^{-n})	n	B_{dir} (s^{-1} K^{-n})	τ_0 (s)	Δ (K)
3	1.6 ± 0.2	5.7 ± 0.1	275 ± 7	–	–
4	–	–	2331 ± 17	(7.3 ± 0.3) × 10^{-10}	31.7 ± 0.2
4b	–	–	89 ± 13 s^{-1}	(3 ± 2) × 10^{-8}	40.6 ± 12
5	11.4 ± 0.2	5.38 ± 0.01	1009 ± 6	–	–

444

445